

# hp-CLOUD APPROXIMATION OF THE DIRAC EIGENVALUE PROBLEM: THE WAY OF STABILITY

HASAN ALMANASREH

**ABSTRACT.** We apply hp-cloud method to the radial Dirac eigenvalue problem. The difficulty of occurrence of spurious eigenvalues among the genuine ones is treated. The method of treatment is based on assuming hp-cloud Petrov-Galerkin scheme to construct the weak formulation of the problem which adds a consistent diffusivity to the variational formulation. The size of the artificially added diffusion term is controlled by a derived stability parameter ( $\tau$ ). The derivation of  $\tau$  considers the limit behavior of the eigenvalues at infinity. The importance of  $\tau$  is of being applicable for generic basis functions. This is together with choosing appropriate intrinsic enrichments in the construction of the cloud shape functions.

## Introduction.

In the last decades, several numerical methods have been derived to compute the eigenvalues of operators. The need of accurate computation of eigenvalues is intensively considered due to their significant applications in many disciplines of science: Mathematically, if a matrix or a linear operator is diagonalized, then by the spectral theorem, it can be analyzed by studying their corresponding eigenvalues, i.e. transforming the matrix or operator to a set of eigenfunctions which can be easily studied. From physical point of view, the eigenvalues could have wide range of information about the behavior of the desired system governed by an operator. This information might be all what is needed to answer many questions regarding the system properties such as stability, positivity, boundedness, asymptotic behavior, etc. Psychologically, one of the brain duties is the processing of visual data, which is mainly treated by the help of eigenvalues. Of course, eigenvalues have the functionality of this biological trait, they convert the abstract notions of operator to the corresponding picture in the complex plane. In mechanics, they play an important role in many branches as determining whether the automobile is noisy, or whether a bridge will collapse by the water waves, etc. Also, the eigenvalues describe how the quantum state of a physical system changes in time (Schrödinger equation). They represent the electron energies in the atomic levels, this is the well-known Dirac equation, which is the core of the present work.

The calculation of energy levels in Helium-like ions, where the interaction between two electrons takes place, can be determined by studying the electrons correlation which is part of

---

*Key words and phrases.* Dirac operator, spurious eigenvalues, meshfree method, clouds, moving least-squares, intrinsic enrichment, Petrov-Galerkin, stability parameter.

Department of Mathematical Sciences and Department of Physics, University of Gothenburg, SE-412 96 Göteborg, Sweden.

quantum electrodynamic (QED) effects. A scheme of calculating QED effects [29, 33, 38, 40] is based on a basis set of relativistic Hydrogen-like ion wave functions (of the Dirac operator). Meanwhile, the numerical computation of the finite basis set of wave functions encounters unphysical values (do not match the physical observations) called spurious eigenvalues or spectrum pollution. The spurious eigenvalues result in rapid oscillations in the wave functions, hence, in many cases, ruining the computation reliability of the basis set (partially or or might be completely) in the practical atomic calculations.

The spurious solution is an effect of the numerical methods and are found in the computational solution of many problems rather than the Dirac equation. For general eigenvalue problems, spurious eigenvalues are reported [46], the occurrence of the spuriousity is related to mismatching of desired properties of the original solution in the numerical formulation. Also in the computation of electromagnetic problems the spuriousity is perceived [34, 39]. In the computation of Dirac eigenvalues, the spuriousity has been reported [1, 2, 37, 41]. Two leading approaches are derived to solve this difficulty completely; Shabaev et al. [41] have related the spuriousity to the same treatment of the large and small Dirac radial functions, their remedy is based on deriving dual kinetic-balance (DKB) basis functions for the large and small components. Almanasreh et al. [2] have allied the occurrence of spurious eigenvalues to the same treatment of the trial and test functions in the finite element method (FEM), they proposed stability scheme based on creating a consistent diffusivity by modifying the test function to include a balanced derivative-correction term.

In this work, we apply hp-cloud method [15, 47] to the radial Dirac equation. The technique is known as one of the meshfree methods (MMs) [6, 18, 30, 31, 35] that allows to two different enrichments, intrinsic and extrinsic, to be built in the construction of the basis functions. The method was previously applied for different problems e.g. Schrödinger equation [10], Mindlin's thick plate model [19], and Timoshenko beam problems [32], etc. Here, in order to treat the spuriousity problem, we stabilize the computation by considering instead hp-cloud Petrov-Galerkin (hp-CPG) method which can be considered as a new technique of the general meshfree local Petrov-Galerkin (MLPG) [4, 17, 28]. The stability scheme is based on adding consistent diffusion terms without deforming the structure of the equation, i.e. the original solution also satisfies the weak formulation. The size of the additional diffusivity is controlled by a derived stability parameter.

Consider the radial Dirac equation  $H_\kappa \Phi(x) = \lambda \Phi(x)$ , where  $\Phi(x) = (F(x), G(x))^t$  is the radial wave function and  $\lambda$  is the electron energy. The weak formulation of the problem is to find  $\lambda \in \mathbb{R}$  and  $\Phi$  in a specified functional space such that for every test function  $\Psi$  living in some suitable space we have  $\int_\Omega \Psi^t H_\kappa \Phi dx = \lambda \int_\Omega \Psi^t \Phi dx$ . The usual hp-cloud Galerkin approximation is to let  $\Psi$  to be  $(\psi, 0)^t$  and  $(0, \psi)^t$  where  $\psi$  lives in the same space as of the two components of  $\Phi$ . To discretize the weak form, the components of the trial function  $\Phi$  and the test function  $\psi$  are chosen from a finite set of hp-cloud basis functions which inherits the properties of the proposed functional space and, is constructed using moving least-squares method on a set of arbitrary nodes in the domain  $\Omega$ . Since the Dirac operator is dominated by advection (convection) terms, hp-cloud approximation will be upset by spurious eigenvalues.

To stabilize hp-cloud approximation, hp-CPG is used instead to formulate the problem. In this formulation, the test function  $\Psi$  is assumed to live in a functional space differs from that of

the trial function  $\Phi$ , i.e.  $\Psi$  is chosen in the form  $(\psi, \tau\psi')^t$  and  $(\tau\psi', \psi)^t$  where  $\psi$  belongs to the same space as the components of  $\Phi$ . The correction term  $\tau\psi'$  is used to add artificial diffusivity to stabilize the convection terms. The size of the diffusion terms is controlled by the stability parameter  $\tau$ . The derivation of  $\tau$  follows the principle used in [2] for FEM, but a generalization of it. Two simplified leading assumptions are considered in deriving  $\tau$ ; the operator limit as the radial variable  $x$  tends to infinity, thus a comparison can be held with the theoretical limit point of eigenvalues, along with considering the dominant terms with respect to the speed of light  $c$ .

The work is organized as follows; in Section 1, some preliminaries about the Dirac equation are presented, also we shed some light on the spuriousity and its causality. In Section 2, the construction of hp-cloud functions is provided, also coupling with FEM to impose essential boundary conditions (EBCs) is explained. hp-CPG and the derivation of the stability parameter are treated in Section 3. In the last section, Section 4, we present some numerical results and provide necessary discussion about the stability scheme.

## 1. THE RADIAL DIRAC EQUATION AND THE PROBLEM OF SPURIOUS EIGENVALUES

The free Dirac space-time equation is

$$(1) \quad i\hbar \frac{\partial}{\partial t} \mathbf{u}(\mathbf{x}, t) = \mathbf{H}_0 \mathbf{u}(\mathbf{x}, t), \quad \mathbf{u}(\mathbf{x}, 0) = \mathbf{u}_0(\mathbf{x}),$$

where  $\hbar$  is the Planck constant divided by  $2\pi$ , and  $\mathbf{H}_0 : H^1(\mathbb{R}^3; \mathbb{C}^4) \longrightarrow L^2(\mathbb{R}^3; \mathbb{C}^4)$  is the free Dirac operator acting on the four-component vector  $\mathbf{u}$ , given by

$$(2) \quad \mathbf{H}_0 = -i\hbar c \boldsymbol{\alpha} \cdot \nabla + mc^2 \beta,$$

where  $m$  is the electron mass, the constant  $c$  is the speed of light, and  $\boldsymbol{\alpha} = (\alpha_1, \alpha_2, \alpha_3)$  and  $\beta$  are the  $4 \times 4$  Dirac matrices given by

$$\alpha_i = \begin{pmatrix} 0 & \sigma_i \\ \sigma_i & 0 \end{pmatrix} \quad \text{and} \quad \beta = \begin{pmatrix} I & 0 \\ 0 & -I \end{pmatrix},$$

$I$  and  $0$  are the  $2 \times 2$  unity and zeros matrices respectively, and  $\sigma_i$ 's are the  $2 \times 2$  Pauli matrices

$$\sigma_1 = \begin{pmatrix} 0 & 1 \\ 1 & 0 \end{pmatrix}, \quad \sigma_2 = \begin{pmatrix} 0 & -i \\ i & 0 \end{pmatrix}, \quad \text{and} \quad \sigma_3 = \begin{pmatrix} 1 & 0 \\ 0 & -1 \end{pmatrix}.$$

Note that separation of variable yields the Dirac eigenvalue problem, i.e. by assuming  $\mathbf{u}(\mathbf{x}, t) = u(\mathbf{x})\theta(t)$  in (1) one gets

$$(3) \quad \mathbf{H}_0 u(\mathbf{x}) = \lambda u(\mathbf{x}).$$

The operator  $\mathbf{H}_0$  is self adjoint on  $H^1(\mathbb{R}^3; \mathbb{C}^4)$ , it describes the motion of the electron that moves freely without external forces. The free Dirac operator with Coulomb potential is read as

$$(4) \quad \mathbf{H} = \mathbf{H}_0 + V(\mathbf{x})I_4,$$

where  $V(\mathbf{x}) = \frac{-Z}{x}$ , and  $I_4$  is the  $4 \times 4$  identity matrix. The spectrum, denoted by  $\sigma$ , of the Coulomb-Dirac operator is  $\sigma(\mathbf{H}) = (-\infty, -mc^2] \cup \{\lambda_k\}_{k \in \mathbb{N}} \cup [mc^2, +\infty)$ , where  $\{\lambda_k\}_{k \in \mathbb{N}}$  is a discrete sequence of eigenvalues in the gap  $(-mc^2, mc^2)$  of the continuous spectrum.

The radial Coulomb-Dirac operator can be obtained by separation of variables in the radial and angular parts, i.e. by assuming  $u(\mathbf{x}) = \frac{1}{x} \begin{pmatrix} F(x)\chi_{\kappa,m}(\varpi, \Theta) \\ iG(x)\chi_{-\kappa,m}(\varpi, \Theta) \end{pmatrix}$ , where  $x$  represents the radial variable. The spherical symmetry property of the angular function  $\chi$  is the key observation point in the derivation of the radial part. Thus, the radial Dirac equation is given as

$$(5) \quad H_\kappa \Phi(x) = \lambda \Phi(x), \text{ where } \Phi(x) = \begin{pmatrix} F(x) \\ G(x) \end{pmatrix} \text{ and}$$

$$(6) \quad H_\kappa = \begin{pmatrix} mc^2 + V(x) & c(-D_x + \frac{\kappa}{x}) \\ c(D_x + \frac{\kappa}{x}) & -mc^2 + V(x) \end{pmatrix}.$$

The radial functions  $F(x)$  and  $G(x)$  are respectively the large and small components of the wave function  $\Phi(x)$ ,  $\lambda$  is the relativistic energy and  $\kappa$  is the spin-orbit coupling parameter defined as  $\kappa = (-1)^{j+\ell+\frac{1}{2}}(j + \frac{1}{2})$ , where  $j$  and  $\ell$  are the total and the orbital angular momentum quantum numbers respectively.

The well-known difficulty of solving the radial Dirac equation numerically is the presence of spurious eigenvalues among the genuine ones that disturb the solution and consequently affect the reliability of the approximated eigenstates. Here we follow [2] for the classification of the spurious eigenvalues; the first category is the so-called instilled spuriousity, and the second category is the unphysical coincidence phenomenon. The first type is those spurious eigenvalues that may occur within the true eigenvalues (i.e. they occur between the true energy levels), this type of spuriousity appears for all values of  $\kappa$ . The second type is the unphysical assigning of almost same first energy for  $2s_{1/2}(\kappa = -1)$  and  $2p_{1/2}(\kappa = 1)$ ,  $3p_{3/2}(\kappa = -2)$  and  $3d_{3/2}(\kappa = 2)$ ,  $4d_{5/2}(\kappa = -3)$  and  $4f_{5/2}(\kappa = 3)$ , and so on. This phenomenon is deeply studied in [42] from theoretical aspect, also, from numerical point of view we refer to [43].

Apparently, most authors [1, 2, 37, 41] agree that the incorrect balancing and the symmetric treatment of the large and small components of the wave function or of the test and trial functions in the numerical methods are the core of the problem. In the present work, we relate the occurrence of spuriousity (for both categories) to the unsuitable functional spaces and to the symmetric treatment of the trial and test functions in the weak formulation of the equation. To clarify, we rewrite (5) to obtain an explicit formula for each of the two radial functions, so by defining  $w^\pm(x) = \pm mc^2 + V(x)$  we have

$$(7) \quad F''(x) + \gamma_1(x, \lambda)F'(x) + \gamma_2(x, \lambda)F(x) = 0,$$

$$(8) \quad G''(x) + \theta_1(x, \lambda)G'(x) + \theta_2(x, \lambda)G(x) = 0,$$

where

$$\gamma_1(x, \lambda) = -\frac{V'(x)}{w^-(x) - \lambda}, \quad \theta_1(x, \lambda) = -\frac{V'(x)}{w^+(x) - \lambda},$$

$$\gamma_2(x, \lambda) = \frac{(w^+(x) - \lambda)(w^-(x) - \lambda)}{c^2} - \frac{\kappa^2 + \kappa}{x^2} - \frac{\kappa V'(x)}{x(w^-(x) - \lambda)},$$

and

$$\theta_2(x, \lambda) = \frac{(w^+(x) - \lambda)(w^-(x) - \lambda)}{c^2} - \frac{\kappa^2 - \kappa}{x^2} + \frac{\kappa V'(x)}{x(w^+(x) - \lambda)}.$$

According to (7) and (8), the components  $F$  and  $G$  should be continuous and have continuous first derivatives. Thus, the suitable choices of functional spaces for the computation of the Dirac eigenvalue problem are those that possessing these properties. Assuming appropriate spaces helps in partial elimination of spurious eigenvalues, and does not help overcoming the coincidence phenomenon. In [2], the same argument is accounted, where FEM is applied to approximate the eigenvalues using linear basis functions

TABLE 1. This table, taken from [2], shows the first computed eigenvalues of the electron in the Hydrogen atom.

Level	$\kappa = 1$	$\kappa = -1$	Rel. Form. $\kappa = -1$
1	-0.50000665661	-0.50000665659	-0.50000665659
2	-0.12500208841	-0.12500208839	-0.12500208018
3	-0.05555631532	-0.05555631532	-0.05555629517
$\Rightarrow$	-0.03141172061	-0.03141172060	Spurious Eigenvalue
4	-0.03118772526	-0.03118772524	-0.03125033803
5	-0.01974434510	-0.01974434508	-0.02000018105

In Table 1, 400 nodal points are used to discretize the domain, and the computation is performed for point nucleus. The shaded left corner value is what meant by the unphysical coincidence phenomenon, and the fourth row elements are the so-called instilled spuriousity. If the basis functions are chosen to be, in addition,  $C^1$  functions, then some instilled spurious eigenvalues are avoided as indicated in [2]. Therefore, after applying the boundary conditions, zero Dirichlet conditions are assumed for both radial functions at the lower and upper boundaries, the proposed space is  $\mathcal{H}(\Omega) := C^1(\Omega) \cap H_0^1(\Omega)$ . Also, the radial functions are mostly-like to vanish at the boundaries in a damping way (except some states), consequently zero Neumann boundary conditions should be taken into account. The exceptional states are  $1s_{1/2}$  and  $2p_{1/2}$ , in this case at the upper boundary the same treatment is considered, but the derivative of these states at the lower boundary is not zero. Here we will assume general boundary conditions, that is, homogeneous Dirichlet boundary conditions. Thus, from now on, the space  $\mathcal{H}(\Omega)$  is considered.

What deserves to dwell upon is that most of numerical methods when they are applied to convection dominant problem the solution is disturbed by unreal oscillations. This instability is getting worse as the convection size increases. The following two numbers are considered as tools to measure the dominance of the convection term

$$(9) \quad Pe_j = \frac{|u_j|h_j}{2K} \quad \text{and} \quad Da_j = \frac{s_j h_j}{|u_j|},$$

where  $Pe_j$  and  $Da_j$  are known as the grid Peclet and Damköhler numbers respectively,  $h_j$  is the size of the element interval  $I_j$ ,  $u_j$  and  $s_j$  are respectively the coefficients of the convection and the reaction terms corresponding to  $I_j$ , and  $K$  is the diffusivity size. The difficulty is addressed when either the convection coefficient or the source term is larger than the diffusive coefficient,

i.e. when  $Pe_j > 1$  or when  $2Pe_j Da_j = \frac{s_j h_j^2}{K} > 1$  respectively, then the associated equation is governed by the convection dominant case.

For the simplified equations (7) and (8), it is easy to check that  $2PeDa$  admits very large values if small number of nodal points is considered regardless the sizes of  $|\lambda|$ ,  $Z$ , and  $\kappa$ . Even with mesh refinement,  $2PeDa$  still admits very large values at some positions ( $2Pe_j Da_j \gg 1$  for some  $j$ ). The Peclet number,  $Pe$ , for the equation that involves the function  $F$ , is always less than 1. But for the equation that corresponds to  $G$ ,  $Pe$  admits a value greater than one, exactly at the nodal point where  $u_j$  changes its sign, here refining the mesh does not bring  $Pe$  below one for all choices of  $\lambda$ ,  $Z$ , and  $\kappa$ . Hence, (7) and (8) are dominated by convection terms. Thus the approximated solutions  $F$  and  $G$ , will be upset by unphysical oscillations. Drawing back, these oscillations in the eigenfunctions result in some unphysical eigenvalues, the spurious eigenvalues. For detailed materials about convection dominant problems we refer to [7, 8].

## 2. MOVING LEAST-SQUARES (MLS) APPROXIMATION

To build hp-cloud functions, moving least-squares (MLS) method is applied which allows easily p-enrichment to be implemented and to desired fundamental characters to be enriched in the approximation. MLS is a well-known approximation technique for constructing meshfree shape functions in general. It applies certain least square approach to get the best local approximation, then the local variable is let to 'move' to cover the whole domain.

Consider an open bounded domain  $\Omega \subset \mathbb{R}$  with boundary  $\partial\Omega$ , assume  $X = \{x_1, x_2, \dots, x_n\}$  is a set of  $n$  arbitrary points in  $\overline{\Omega}$ . Let  $W$  be a set of open covering of  $\Omega$  defined by  $X$  such that  $W = \{w_i\}_{i=1}^n$  where  $w_i$  is centered at  $x_i$  and  $\Omega \subset \cup_{i=1}^n w_i$ .

**Definition 1.** A set of functions  $\{\psi_i\}_{i=1}^n$  is called a partition of unity (PU) subordinated to the cover  $W$  if

- (1)  $\sum_{i=1}^n \psi_i(x) = 1$ , for all  $x \in \Omega$ .
- (2)  $\psi \in C_0^s(w_i)$ , for  $i = 1, 2, \dots, n$ , where  $s \geq 0$ .

Let  $P = \{p_1(x), p_2(x), \dots, p_m(x)\}$  be a set of basis of polynomials (or any basis of suitable intrinsic enrichments). Suppose that  $\Psi(x)$  is a continuous function defined on  $\Omega$  and that its values,  $\Psi_i$ , at the points  $x_i \in \overline{\Omega}$ ,  $i = 1, 2, \dots, n$ , are given. To approximate  $\Psi(x)$  globally by  $\Psi_h(x)$ , firstly  $\Psi(x)$  is approximated locally at  $\tilde{x} \in \overline{\Omega}$  by  $J_{\tilde{x}}\Psi$  defined in terms of the given basis set  $P$  as

$$(10) \quad J_{\tilde{x}}\Psi(x) = P^t(x)a(\tilde{x}),$$

where  $t$  denotes for the usual transpose. The unknown coefficients  $a(\tilde{x})$  are chosen so that  $J_{\tilde{x}}\Psi$  is the best approximation of  $\Psi$  in a certain least squares sense, this is achieved if  $a$  is selected to minimize the following weighted least squares  $L^2$ -error norm

$$(11) \quad I_{\tilde{x}}(a) = \sum_{i=1}^n \varphi_i\left(\frac{x - x_i}{\rho_i}\right)(P^t(x_i)a(\tilde{x}) - \Psi_i)^2,$$

where  $\varphi_i$  are the weight functions introduced to insure the locality of the approximation, and  $\rho_i$  are the dilation parameters which control the support radius of  $\varphi_i$  at  $x_i$ . To minimize  $I_{\tilde{x}}$  with

respect to the vector  $a$ , the first derivative test is applied, i.e. we set  $\frac{\partial I_{\tilde{x}}}{\partial a} = 0$  which gives

$$\begin{aligned}\frac{\partial I_{\tilde{x}}}{\partial a_1} &= \sum_{i=1}^n \varphi_i \left( \frac{x-x_i}{\rho_i} \right) 2p_1(x_i) (P^t(x_i)a(\tilde{x}) - \Psi_i) = 0. \\ \frac{\partial I_{\tilde{x}}}{\partial a_2} &= \sum_{i=1}^n \varphi_i \left( \frac{x-x_i}{\rho_i} \right) 2p_2(x_i) (P^t(x_i)a(\tilde{x}) - \Psi_i) = 0. \\ &\vdots \\ \frac{\partial I_{\tilde{x}}}{\partial a_m} &= \sum_{i=1}^n \varphi_i \left( \frac{x-x_i}{\rho_i} \right) 2p_m(x_i) (P^t(x_i)a(\tilde{x}) - \Psi_i) = 0.\end{aligned}$$

The above system can be written as

$$(12) \quad M(x)a(\tilde{x}) - B(x)\Psi = 0,$$

where  $M(x) = \mathcal{P}^t \Upsilon(x) \mathcal{P}$ ,  $B(x) = \mathcal{P}^t \Upsilon(x)$ ,  $\Psi^t = [\Psi_1, \Psi_2, \dots, \Psi_n]$ ,  $a^t(\tilde{x}) = [a_1(\tilde{x}), a_2(\tilde{x}), \dots, a_m(\tilde{x})]$ , and  $\mathcal{P}$  and  $\Upsilon(x)$  are defined respectively as

$$\mathcal{P} = \begin{pmatrix} p_1(x_1) & p_2(x_1) & \dots & p_m(x_1) \\ p_1(x_2) & p_2(x_2) & \dots & p_m(x_2) \\ \vdots & \vdots & \ddots & \vdots \\ p_1(x_n) & p_2(x_n) & \dots & p_m(x_n) \end{pmatrix}$$

and

$$\Upsilon(x) = \begin{pmatrix} \varphi_1\left(\frac{x-x_1}{\rho_1}\right) & 0 & \dots & 0 \\ 0 & \varphi_2\left(\frac{x-x_2}{\rho_2}\right) & \dots & 0 \\ \vdots & \vdots & \ddots & \vdots \\ 0 & 0 & \dots & \varphi_n\left(\frac{x-x_n}{\rho_n}\right) \end{pmatrix}.$$

We proceed from equation (12) to get

$$(13) \quad a(\tilde{x}) = M^{-1}(x)B(x)\Psi.$$

Thus

$$\begin{aligned}J_{\tilde{x}}\Psi(x) &= P^t(x)a(\tilde{x}) \\ &= P^t(x)M^{-1}(x)B(x)\Psi.\end{aligned}$$

The global approximations is then obtained by assuming  $\tilde{x}$  arbitrary, i.e. by letting  $\tilde{x}$  move over the domain, viz, the solution is globalized by considering  $\Psi(x) \approx \lim_{\tilde{x} \rightarrow x} J_{\tilde{x}}\Psi(x) =: \Psi_h(x)$ , thus

$$(14) \quad \Psi_h(x) = \sum_{i=1}^n \psi_i(x)\Psi_i$$

with  $\psi_i(x) = P^t(x)M^{-1}(x)B_i(x)$ , and  $B_i(x) = \varphi_i\left(\frac{x-x_i}{\rho_i}\right)P(x_i)$ . In the sum form  $\Psi_h$  is written as

$$(15) \quad \Psi_h(x) = P^t(x) \left( \sum_{i=1}^n \varphi_i \left( \frac{x-x_i}{\rho_i} \right) P(x_i) P^t(x_i) \right)^{-1} \sum_{i=1}^n \varphi_i \left( \frac{x-x_i}{\rho_i} \right) P(x_i) \Psi_i.$$



The first derivative of  $\psi_i$  is given as  $\psi_{i,x} = \frac{d\psi_i(x)}{dx} = P_x^t M^{-1} B_i - P^t M^{-1} M_x M^{-1} B_i + P^t M^{-1} B_{i,x}$ . To increase the order of consistency (a set of functions  $\{u_i(x)\}$  is consistent of order  $m$  if  $\sum_{i=1}^m u_i(x) \mathfrak{P}(x_i) = \mathfrak{P}(x)$  for all  $x \in \Omega$ , where  $\mathfrak{P}(x) = \{x^\varsigma; |\varsigma| \leq m\}$ ) of the approximation, the complete representation of the hp-cloud functions consists of the set of PU functions  $\psi_i(x)$  and monomial extrinsic enrichment basis functions  $P$  as

$$\begin{aligned} \Psi_h(x) &= \sum_{i=1}^n \psi_i(x) \left( \sum_{j=1}^{n_0} P_j(x) \Psi_i^j \right) \\ &= \sum_{i=1}^n \sum_{j=1}^{n_0} \psi_i(x) P_j(x) \Psi_i^j. \end{aligned}$$

Note that  $P$  is chosen to be a set of monomials, also it can be other types of basis functions, but the most used choice is monomials since they provide good approximation for smooth functions. The monomials  $P_j(x)$ , according to [47], should be normalized by the measure of the grid size at  $x_j$  to prevent numerical instability. Nevertheless, in applying hp-cloud approximation for the Dirac eigenvalue problem, we will use a stability scheme based on MLPG method, for that we will not be interested in concerning extrinsic enrichments in the computation ( $P = \{1\}$ , a monomial of degree zero). The point of this setting follows [4], where six different realizations of MLPG restricted only to intrinsic enrichment basis are considered. It is found that extrinsic enrichment in MLPG causes numerical stability problems, because the behavior of their derivatives has large oscillations, which is not the case in the usual MMs. Hence, in the present work, only intrinsic enrichments,  $P(x)$ , are considered, and thus the approximation with hp-clouds is given by (14).

The weight functions  $\varphi_i$  play the most important role in hp-cloud shape function definition, they are defined locally on the covers  $w_i$  around  $x_i$ . The functions  $\varphi_i$  can also be chosen the same for all nodes, in this case we write  $\varphi_i = \varphi$ , which is the case assumed in this work. The hp-clouds,  $\psi_i$ , inherit the properties of the weight function  $\varphi$  such as continuity, smoothness, and others. I.e. if  $\varphi$  is continuous with continuous derivatives, then so are  $\psi_i$ , provided that the continuity of the enrichment basis  $P(x)$  and its derivatives is ensured. As for the Dirac large and small components,  $F$  and  $G$ , the proposed space is  $\mathcal{H}$ , thus, and therefore, the weight function  $\varphi$  should be at least  $C^1$ -function. For this purpose, we will consider quartic splines (which are  $C^2$ , sufficiently enough) as weight functions defined as

$$(16) \quad \varphi(r) = \begin{cases} 1 - 6r^2 + 8r^3 - 3r^4, & r \leq 1, \\ 0, & r > 1, \end{cases}$$

where  $r = \frac{|x-x_i|}{\rho_i}$ .

The set functions  $\{\psi_i\}_{i=1}^n$  builds a PU, also the set of their derivatives  $\{\psi_{i,x}\}_{i=1}^n$  builds a partition of nullity (PN) ( $\sum_{i=1}^n \psi_{i,x}(x) = 0$  for all  $x \in \Omega$ ), see Figure 1. The computational effort of evaluating integrals in the weak form in hp-cloud approximation is more time consuming compared to mesh-based methods (the shape functions are of the form  $\varphi_i$  only), this is due to the fact that the derivative of the shape function  $\psi_i$  tends to have non-polynomial characters, also due to the time needed for matrix inversion in evaluating the shape functions.



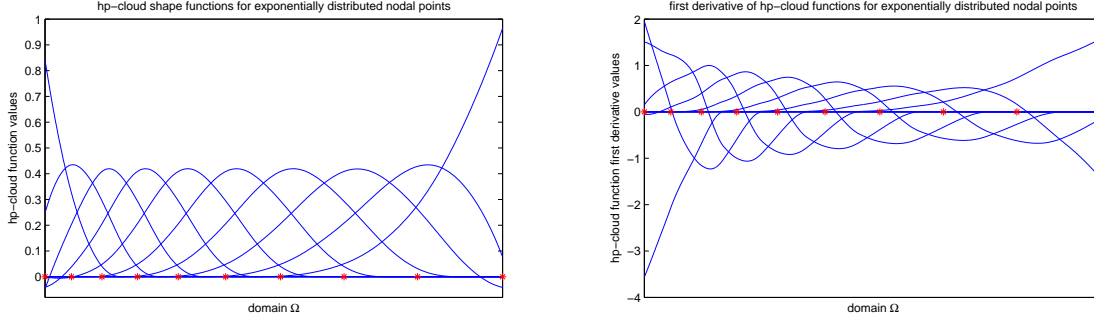


FIGURE 1. PU hp-clouds (to the left) and their PN first derivatives (to the right). Quartic splines are used as weight functions.

Since the Kronecker delta property is not being a character of  $\psi_i$  ( $\psi_i(x_j) \neq \delta_{ij}$ ), then at each node there are at least two nonzero shape functions. Thus, to have the value of the approximated function at a node, all nonzero shape functions effect should be added. The missing of this property causes a problem in imposing essential boundary conditions, and thus other techniques are used to solve this difficulty, this is coming soon.

The intrinsic enrichment  $P(x)$  has an important effect in the approximation definition. All known fundamental characters such as discontinuities and singularities about the sought solution can be loaded on the intrinsic functions. Consequently, more time is saved (it is not needed, in general, to assume very large nodal points to capture a desired behavior of the approximated function while most of the solution features are inserted in the approximation itself), on the other hand, stability is enhanced particularly when there are some crucial characters that can not be captured by usual numerical methods, for example solving the equations with rough coefficients that appear e.g. in composites and materials with micro-structure, or problems with high oscillatory solutions, or eigenvalue problems that admit spurious eigenvalues in the computation of the discrete spectrum.

### Imposition of essential boundary conditions (EBCs).

The Dirac eigenvalue problem assumes homogeneous EBCs, while it is known that hp-cloud approximation (MMS in general) can not treat these conditions naturally, this because, as it is mentioned before, the lack of the Kronecker delta property of the shape function. This is in contrast with most mesh-based methods, where the basis set functions admits this property, and thus applying these boundary conditions is straightforward (as in FEM) by omitting the first and the last basis functions.

In MMs in general, the widely applied techniques for imposing EBCs are Lagrangian multipliers, penalty condition, and coupling with finite element shape functions. Lagrangian multiplier is a general approach and provides good results. The disadvantage of this technique, see e.g. [18, 45], is that the result discrete equations for a self-adjoint operator are not positive definite

(contains zero at the main diagonal) nor banded, also the structure of the system becomes awkward, i.e. instead of having  $\mathcal{M}$  as a result matrix of the computations, the system  $\begin{pmatrix} \mathcal{M} & Lm \\ Lm & 0 \end{pmatrix}$  is obtained, where  $Lm$  is the EBC-enforcement vector. EBCs can also be imposed by penalty condition [18, 36], the problem of applying this technique is the negative effect on the condition number of the resulting discrete equations.

The most powerful and safe method to enforce EBCs is coupling MMs with FEM, known for first time by [26]. With this approach, the meshfree shape functions of the nodes along boundaries are replaced by finite element basis functions. In one dimensional case, hp-cloud functions at the first two and last two nodes are replaced by finite element functions, and imposing EBCs, as the usual way in FEM, is simply by eliminating the first and the last added FEM functions, see Figure 2.

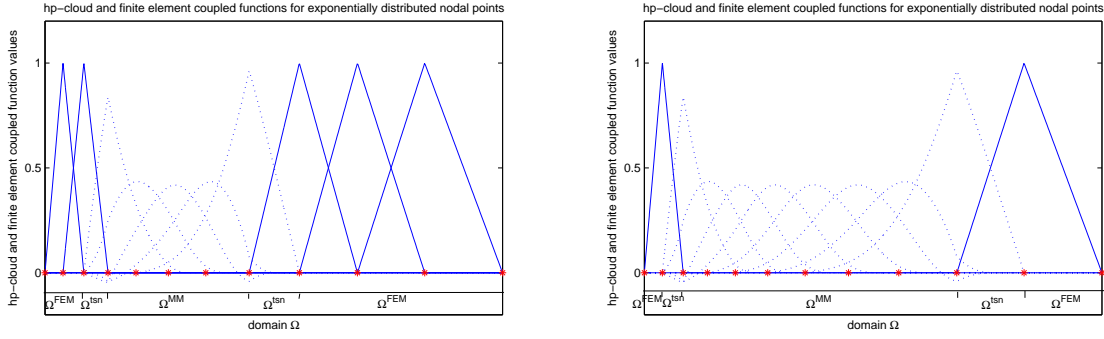


FIGURE 2. Coupled hp-cloud and finite element functions: general coupling (to the left), and coupling for the purpose of imposing EBCs (to the right) (two finite element shape functions are sufficient). Linear (hat) functions are used as finite element functions, and quartic splines as weight functions in the hp-clouds.

Two efficient ways of coupling MMs with FEM; coupling with a Ramp function [5]. In this approach the derivative of the resulting coupled approximation function along the nodes in the interface region is discontinuous and the consistency is of first order. To ensure the continuity of the derivative of the coupled function and to obtain consistency of any order, we consider the second type; coupling with reproducing conditions [23]. Using MLS approximation method as before, the coupled hp-cloud and finite element functions with the reproducing conditions type are given as (see e.g. [18])

$$\begin{aligned} \Psi_h(x) &= \sum_{x_i \in \Omega^{MM}} \psi_i(x) \Psi_i + \sum_{x_i \in \Omega^{FEM}} \mathcal{G}_i(x) \Psi_i \\ &= \sum_{x_i \in \Omega^{MM}} \left( P^t(x) - \sum_{x_i \in \Omega^{FEM}} \mathcal{G}_i(x) P^t(x_i) \right) M^{-1} \varphi_i \left( \frac{x - x_i}{\rho_i} \right) P(x_i) \Psi_i + \sum_{x_i \in \Omega^{FEM}} \mathcal{G}_i(x) \Psi_i, \end{aligned}$$

where  $\mathcal{G}_i$  are the finite element shape functions, and  $M$  is as defined before. From Figure 2, it can be seen that finite element functions are only complete in  $\Omega^{FEM}$ , and that in  $\Omega^{MM}$  only hp-clouds are present. In the transition interface region,  $\Omega^{tsn}$ , the existence of incomplete finite

element functions modifies the exist hp-clouds there, and thus coupled hp-clouds and finite element functions are obtained.

### 3. THE SCHEME AND THE STABILITY PARAMETER

Since the Dirac equation is dominated by convection terms, hp-cloud method will be unstable. As most of numerical methods where their modifications are used to stabilize solutions [2, 3, 7, 8, 12, 25], instead of considering hp-cloud method, we will apply hp-CPG technique to create diffusion terms to stabilize the approximation. hp-CPG is a consistent method in the sense that the solution of the original problem is also a solution to the weak form. The size of the added diffusivity is controlled by a stability parameter. To set the scheme, consider the radial Dirac equation  $H_\kappa \Phi = \lambda \Phi$ , the usual hp-cloud method is formalized by multiplying this equation by a test function  $\Psi$  and integrate over the domain  $\Omega$

$$(17) \quad \int_{\Omega} \Psi^t H_\kappa \Phi dx = \lambda \int_{\Omega} \Psi^t \Phi dx.$$

To discretize (17) let  $\Psi$  be  $(\psi_i, 0)^t$  and  $(0, \psi_i)^t$  where  $i = 1, 2, \dots, n$ , and

$$(18) \quad \Phi(x) = \begin{pmatrix} F(x) \\ G(x) \end{pmatrix} = \begin{pmatrix} \Phi^F := \sum_{j=1}^n f_j \psi_j(x) \\ \Phi^G := \sum_{j=1}^n g_j \psi_j(x) \end{pmatrix},$$

the elements  $f_j$  and  $g_j$  are the nodal values of  $F$  and  $G$  respectively, and  $\psi_j$  are the hp-cloud basis functions. This yields

$$(19) \quad \sum_{j=1}^n (w^+(x) \psi_j(x), \psi_i(x)) f_j + \sum_{j=1}^n (-c \psi_j'(x) + \frac{c\kappa}{x} \psi_j(x), \psi_i(x)) g_j = \lambda \sum_{j=1}^n (\psi_j(x), \psi_i(x)) f_j$$

and

$$(20) \quad \sum_{j=1}^n (c \psi_j'(x) + \frac{c\kappa}{x} \psi_j(x), \psi_i(x)) f_j + \sum_{j=1}^n (w^-(x) \psi_j(x), \psi_i(x)) g_j = \lambda \sum_{j=1}^n (\psi_j(x), \psi_i(x)) g_j,$$

the bracket  $(\cdot, \cdot)$  is the usual  $L^2(\Omega)$  scalar product. After simplifying, equations (19) and (20) lead to the symmetric generalized eigenvalue problem

$$(21) \quad AX = \lambda BX.$$

The block matrices  $A$  and  $B$  are defined by

$$(22) \quad A = \left( \begin{array}{c|c} mc^2 M_{000} + M_{000}^V & -c M_{010} + c\kappa M_{001} \\ \hline c M_{010} + c\kappa M_{001} & -mc^2 M_{000} + M_{000}^V \end{array} \right), \text{ and } B = \left( \begin{array}{c|c} M_{000} & 0 \\ \hline 0 & M_{000} \end{array} \right),$$

where  $M_{rst}^q$  are  $n \times n$  matrices given as

$$(23) \quad (M_{rst}^q)_{ij} = \int_{\Omega} \psi_j^{(s)} \psi_i^{(r)} x^{-t} q(x) dx, \quad (\psi^{(r)}(x) = \frac{d^r}{dx^r} \psi(x)).$$

The vector  $X$  is the unknown defined as  $(f, g)^t$ , where  $f = (f_1, f_2, \dots, f_n)$  and  $g = (g_1, g_2, \dots, g_n)$ .

To formulate hp-CPG, the test function  $\Psi$  is modified to include the first derivative of the basis function to introduce the required diffusivity. This leads to assume  $\Psi$  as  $(\psi, \tau \psi')^t$  and

$(\tau\psi', \psi)^t$  in (17), where  $\tau$  is the stability parameter that controls the size of the diffusion terms,  $\psi = \psi_i$ , and the functions  $F$  and  $G$  are given as above, thus we get

$$(24) \quad (w^+ F, \psi) + (-cG' + \frac{c\kappa}{x}G, \psi) + (Re^2(F, G), \tau\psi') = \lambda(F, \psi)$$

and

$$(25) \quad (cF' + \frac{c\kappa}{x}F, \psi) + (w^- G, \psi) + (Re^1(F, G), \tau\psi') = \lambda(G, \psi),$$

The functionals  $Re^1(F, G)(x)$  and  $Re^2(F, G)(x)$  are the residuals of the Dirac two-equation system defined as

$$(26) \quad Re^1(F, G)(x) = (W^+ F - cG' + \frac{c\kappa}{x}G)(x),$$

$$(27) \quad Re^2(F, G)(x) = (W^- G + cF' + \frac{c\kappa}{x}F)(x),$$

where  $W^\pm(x) = w^\pm(x) - \lambda$ . This results in the usual hp-cloud approximation with addition to perturbations sized by  $\tau$  as follows

$$(28) \quad \mathbf{A}X = \lambda\mathbf{B}X.$$

The perturbed block matrices,  $\mathbf{A}$  and  $\mathbf{B}$ , are respectively in the forms  $\mathbf{A} = A + \tau\mathcal{A}$  and  $\mathbf{B} = B + \tau\mathcal{B}$ , where  $A$  and  $B$  are given by (22), and

$$(29) \quad \mathcal{A} = \left( \begin{array}{c|c} cM_{110} + c\kappa M_{101} & -mc^2 M_{100} + M_{100}^V \\ \hline mc^2 M_{100} + M_{100}^V & -cM_{110} + c\kappa M_{101} \end{array} \right), \text{ and } \mathcal{B} = \left( \begin{array}{c|c} 0 & M_{100} \\ \hline M_{100} & 0 \end{array} \right).$$

The system above is not symmetric, thus some complex eigenvalues may appear if the size of  $\tau$  is relatively large. In the FEM case, an explicit representation for  $\tau$  can be obtained [2], where the basis functions have the Kronecker delta property, hence the basis functions have regular distribution along the domain and only the adjacent basis functions intersect in one and only one subinterval. Thus the result system consists of tridiagonal matrices, which makes the derivation of  $\tau$  easier and an explicit representation is possible. In meshfree methods in general, the basis function is represented by cloud over the nodal point, with domain of influence,  $\rho$ , that may cover many nodal points. So the result matrices can be filled with many nonzero elements, hence the number of diagonals in the matrices is arbitrary (greater than 3) depending on the size of  $\rho$ . Therefore we can not write explicit representation that depends only and completely on a given mesh (where no mesh is assumed) for  $\tau$ . Instead,  $\tau$  will be mainly represented by some of the computed matrices obtained from the usual hp-cloud method.

The derivation of  $\tau$  assumes the limit Dirac operator in the vicinity of  $x$  at infinity. This presumable simplification is inevitable and justifiable; the derivation leads to an approximation of the limit point eigenvalue which depends on  $\tau$ , where, by [20], information about the theoretical limit is available, hence we can minimize the error between the theoretical and the approximated limits to get  $\tau$ . By considering the limit operator at infinity, we consider the troublesome part (that includes the convection terms) of the operator which is mostly needed to be stabilized. Besides that, one is obliged to assume that the stability parameter should be applicable at all radial positions  $x$ , particularly the large values.

**Theorem 1.** Let  $M_{000}$  and  $M_{100}$  be the  $n \times n$  computed matrices in the generalized system (22), and let  $\sigma_{ji}$  and  $\eta_{ji}$  be the corresponding entries respectively. Define  $\vartheta$  as

$$\vartheta_{ji} = \begin{cases} -\sum_{k=i+1}^j h_k, & i < j, \\ 0, & i = j, \\ \sum_{k=j+1}^i h_k, & i > j, \end{cases}$$

where  $h_k$  is the displacement between the nodes  $x_k$  and  $x_{k-1}$ . Then the stability parameter,  $\tau_j$ , for an arbitrary  $j^{\text{th}}$  row of the matrices in  $\mathcal{A}$  and  $\mathcal{B}$  is given by

$$(30) \quad \tau_j = \left| \sum_{i=1}^n \sigma_{ji} \vartheta_{ji} / \sum_{i=1}^n \eta_{ji} \vartheta_{ji} \right|.$$

Proof. Consider the limit operator of the Dirac eigenvalue problem in the vicinity of  $x$  at infinity

$$(31) \quad \begin{pmatrix} mc^2 & -cD_x \\ cD_x & -mc^2 \end{pmatrix} \begin{pmatrix} F(x) \\ G(x) \end{pmatrix} = \lambda \begin{pmatrix} F(x) \\ G(x) \end{pmatrix}.$$

The hp-CPG variational formulation of (31) (which is equivalent to assume a limit passage as  $x \rightarrow \infty$  of the equations (24) and (25)) provides

$$(32) \quad (mc^2 - \lambda)M_{000}f + \tau c M_{110}f - (\tau mc^2 - c + \tau \lambda)M_{100}g = 0$$

and

$$(33) \quad (\tau mc^2 - c - \tau \lambda)M_{100}f - \tau c M_{110}g - (mc^2 + \lambda)M_{000}g = 0,$$

where, as defined before,  $f = (f_1, f_2, \dots, f_n)$  and  $g = (g_1, g_2, \dots, g_n)$ . Let  $\sigma_k$ ,  $\eta_k$ , and  $\varrho_k$ , for  $k = 1, 2, \dots, n$ , be the corresponding  $j^{\text{th}}$  row entries of  $M_{000}$ ,  $M_{100}$ , and  $M_{110}$  respectively. To obtain  $\tau_j$ , we consider the  $j^{\text{th}}$  row in (32) and (33), this together with the lemma below give

$$(34) \quad (mc^2 - \lambda) \left( \sum_{k=1}^n \sigma_k f_j + \sum_{k=1}^n \sigma_k (mc\vartheta_k + (\vartheta_k/c)\lambda) g_j \right) + \tau c \left( \sum_{k=1}^n \varrho_k f_j + \sum_{k=1}^n \varrho_k (mc\vartheta_k + (\vartheta_k/c)\lambda) g_j \right) - (\tau mc^2 - c + \tau \lambda) \left( \sum_{k=1}^n \eta_k g_j + \sum_{k=1}^n \eta_k (mc\vartheta_k - (\vartheta_k/c)\lambda) f_j \right) = 0$$

and

$$(35) \quad (\tau mc^2 - c - \tau \lambda) \left( \sum_{k=1}^n \eta_k f_j + \sum_{k=1}^n \eta_k (mc\vartheta_k + (\vartheta_k/c)\lambda) g_j \right) - \tau c \left( \sum_{k=1}^n \varrho_k g_j + \sum_{k=1}^n \varrho_k (mc\vartheta_k - (\vartheta_k/c)\lambda) f_j \right) - (mc^2 + \lambda) \left( \sum_{k=1}^n \sigma_k g_j + \sum_{k=1}^n \sigma_k (mc\vartheta_k - (\vartheta_k/c)\lambda) f_j \right) = 0.$$

**Lemma 1.** *Let  $f_i$  and  $g_i$  be respectively the  $i^{\text{th}}$  nodal values of  $F$  and  $G$  of the limit equation (31). Freeze  $j$ , and let  $\vartheta_i$  be given as in the theorem above for the given  $j$ . Then for  $i = 1, 2, \dots, n$*

$$\begin{aligned} f_i &\cong f_j + \left( mc\vartheta_i + (\vartheta_i/c)\lambda \right) g_j. \\ g_i &\cong g_j + \left( mc\vartheta_i - (\vartheta_i/c)\lambda \right) f_j. \end{aligned}$$

Proof. Consider the limit equation (31) which can be written as

$$(36) \quad mc^2 F(x) - cG'(x) = \lambda F(x) \text{ and } cF'(x) - mc^2 G(x) = \lambda G(x).$$

If  $i = j$ , then the result is obvious. So let  $i \neq j$ , we treat the case  $i < j$ , where the proof for  $i > j$  goes through mutatis mutandis by using forward difference approximations for derivatives. Assume  $i < j$ , also we prove the first argument of the lemma, the proof of the second argument is similar. Consider the second part of (36) for  $x_j$

$$(37) \quad cF'(x_j) - mc^2 G(x_j) = \lambda G(x_j).$$

Using backward difference approximations for derivatives we can write

$$(38) \quad F'|_{x_j} \cong \frac{F(x_j) - F(x_i)}{-\sum_{k=i+1}^j h_k} = \frac{f_j - f_i}{-\sum_{k=i+1}^j h_k}.$$

Substituting (38) in (37) completes the proof. ■

We consider the dominant parts with respect to  $c$ , so let  $c \rightarrow \infty$  in (34) and (35) and simplify to get

$$(39) \quad \left[ \sum_{k=1}^n \left( (-\sigma_k - \eta_k \vartheta_k) \lambda + (c\varrho_k - m^2 c^3 \eta_k \vartheta_k) \tau_j + (mc^2 \sigma_k + mc^2 \eta_k \vartheta_k) \right) \right] f_j + \\ + \left[ \sum_{k=1}^n \left( (\tau_j \varrho_k \vartheta_k - \tau_j \eta_k) \lambda + (mc^2 \varrho_k \vartheta_k - mc^2 \eta_k) \tau_j + (m^2 c^3 \sigma_k \vartheta_k + c\eta_k) \right) \right] g_j = 0$$

and

$$(40) + \left[ \sum_{k=1}^n \left( (-\tau_j \eta_k + \tau_j \varrho_k \vartheta_k) \lambda + (mc^2 \eta_k - mc^2 \varrho_k \vartheta_k) \tau_j + (-c\eta_k - m^2 c^3 \sigma_k \vartheta_k) \right) \right] f_j + \\ + \left[ \sum_{k=1}^n \left( (-\eta_k \vartheta_k - \sigma_k) \lambda + (m^2 c^3 \eta_k \vartheta_k - c\varrho_k) \tau_j + (-mc^2 \eta_k \vartheta_k - mc^2 \sigma_k) \right) \right] g_j = 0.$$

To make the derivation simpler, the following notations are introduced

$$\begin{aligned} a &= \sum_{k=1}^n a_k = \sum_{k=1}^n (-\sigma_k - \eta_k \vartheta_k), & b &= cb_1 - m^2 c^3 b_2 = \sum_{k=1}^n (c\varrho_k - m^2 c^3 \eta_k \vartheta_k), \\ d &= mc^2 d_1 = \sum_{k=1}^n mc^2 (\sigma_k + \eta_k \vartheta_k), & e &= \sum_{k=1}^n e_k = \sum_{k=1}^n (\varrho_k \vartheta_k - \eta_k), \\ q &= mc^2 q_1 = \sum_{k=1}^n mc^2 (\varrho_k \vartheta_k - \eta_k), & \omega &= m^2 c^3 \omega_1 + c\omega_2 = \sum_{k=1}^n (m^2 c^3 \sigma_k \vartheta_k + c\eta_k). \end{aligned}$$

By these notations, equations (39) and (40) can be written as

$$(41) \quad \begin{pmatrix} a\lambda + b\tau_j + d & e\tau_j\lambda + q\tau_j + \omega \\ e\tau_j\lambda - q\tau_j - \omega & a\lambda - b\tau_j - d \end{pmatrix} \begin{pmatrix} f_j \\ g_j \end{pmatrix} = \begin{pmatrix} 0 \\ 0 \end{pmatrix}.$$

Since  $f_j$  and  $g_j$  are not identically zero for all  $j$ , then we expect

$$(42) \quad \det \begin{pmatrix} a\lambda + b\tau_j + d & e\tau_j\lambda + q\tau_j + \omega \\ e\tau_j\lambda - q\tau_j - \omega & a\lambda - b\tau_j - d \end{pmatrix} = 0,$$

where  $\det(\cdot)$  is the determinant of matrix. After simplifying, equation (42) leads to

$$(43) \quad \lambda_{\pm}(\tau_j) = \pm \sqrt{\frac{(b\tau_j + d)^2 - (q\tau_j + \omega)^2}{a^2 - e^2\tau_j^2}}.$$

By [20], the only accumulation point for the eigenvalue for the radial Coulomb-Dirac operator in the vicinity of  $x$  at infinity is  $mc^2$ . So, we like to have

$$\begin{aligned} |\lambda_+ - mc^2| &= 0 \\ \iff m^2c^4(a^2 - e^2\tau_j^2) &= (b\tau_j + d)^2 - (q\tau_j + \omega)^2 \\ &= (cb_1\tau_j - m^2c^3b_2\tau_j + mc^2d_1)^2 - (mc^2q_1\tau_j + m^2c^3\omega_1 + c\omega_2)^2. \end{aligned}$$

Letting  $m = 1$ , dividing both sides by  $c^6$ , and taking the limit as  $c \rightarrow \infty$ , we get

$$(44) \quad b_2^2\tau_j^2 - \omega_1^2 = 0.$$

Substituting back the values of  $b_2$  and  $\omega_1$ , the desired consequence is obtained for the fixed  $j$  as

$$(45) \quad \tau_j = \left| \sum_{k=1}^n \sigma_k \vartheta_k / \sum_{k=1}^n \eta_k \vartheta_k \right|.$$

The above result can be generalized for arbitrary  $j$  as

$$(46) \quad \tau_j = \left| \sum_{i=1}^n \sigma_{ji} \vartheta_{ji} / \sum_{i=1}^n \eta_{ji} \vartheta_{ji} \right|,$$

and this ends the proof. ■

The hp-cloud functions depend strongly on the dilation parameter  $\rho_j$ . As  $\rho_j$  getting smaller and smaller, i.e.  $\rho_j \rightarrow \max\{h_j, h_{j+1}\}$  ( $= h_{j+1}$  for exponentially distributed nodal points), the shape functions of MLS in general become more and more equal to the standard FEM functions, see Figure 3. In this case the FEM stability parameter might be applicable for MMs [17]

$$\tau_j^{FEM} \rightarrow \tau_j^{MMs}, \quad \text{as } \rho_j \rightarrow h_{j+1}.$$

On the other hand, one should be careful about the invertibility of the matrix  $M$ , i.e. we can not approach  $\rho_j = h_{j+1}$  which makes  $M$  singular. In Lemma 2, we derive the stability parameter for the computation of the eigenvalues of the Dirac operator,  $H_\kappa$ , using FEM with quartic spline. The proof of the lemma is simple and uses the same technique as of the theorem above, thus we utilize the result of this theorem with minor modifications. In Table 7, the result of applying  $\tau_j^{FEM}$  for stabilizing hp-cloud method with  $\rho_j = 1.1 \cdot h_{j+1}$  is obtained, the approximation is good enough and the spuriousity seems to be eliminated. But a difficulty arises, that is, the end of the spectrum (the spectrum tail) behaves in a strange way, which may be regarded as spurious solutions.



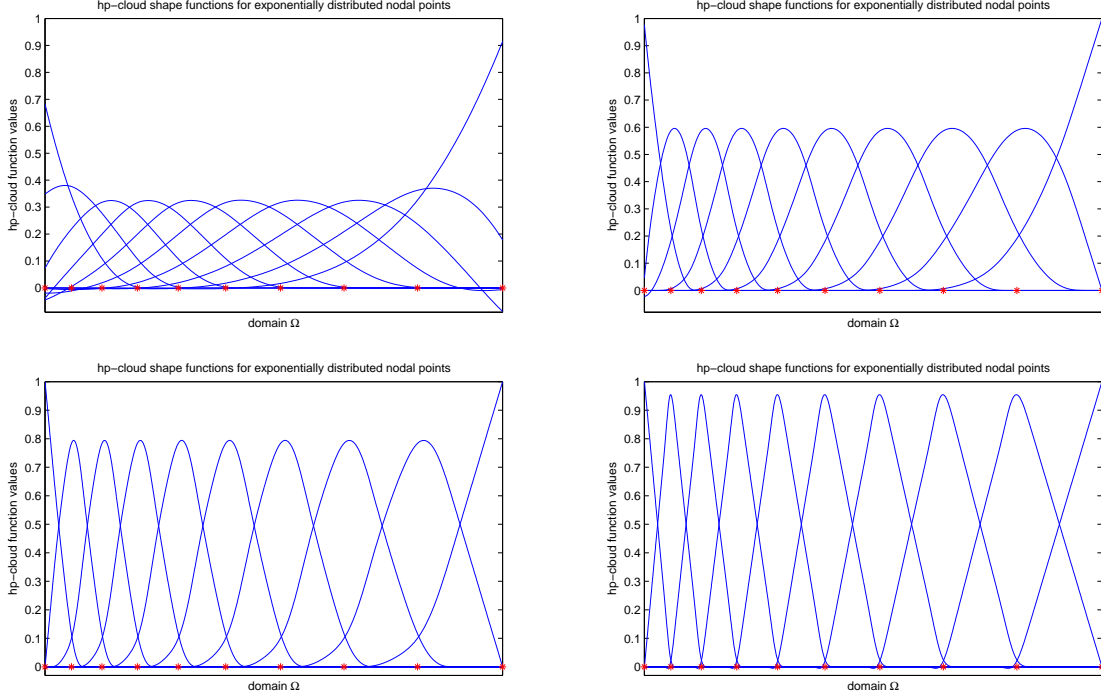


FIGURE 3. PU hp-clouds with different domains of influence:  $\rho_j = 4 \cdot h_{j+1}$  (up to the left),  $\rho_j = 2 \cdot h_{j+1}$  (up to the right),  $\rho_j = 1.5 \cdot h_{j+1}$  (below to the left), and  $\rho_j = 1.2 \cdot h_{j+1}$  (below to the right). Quartic splines are used as weight functions.

**Lemma 2.** *The FEM stability parameter for the computation of the Dirac eigenvalues using quartic splines as a basis has the form*

$$(47) \quad \tau_j^{FEM} = \frac{3}{17} h_{j+1} \frac{(h_{j+1} - h_j)}{(h_{j+1} + h_j)}.$$

Proof. Consider the general formula derived in Theorem 1

$$(48) \quad \tau_j = \left| \sum_{i=1}^n \sigma_{ji} \vartheta_{ji} / \sum_{i=1}^n \eta_{ji} \vartheta_{ji} \right|,$$

where  $\vartheta_{ji}$  is as defined above, and  $r_{ji}$  and  $t_{ji}$  are respectively the  $j^{th}$  row elements of  $M_{000}$  and  $M_{100}$ . Note that in FEM with quartic spline basis functions,  $M_{000}$  and  $M_{100}$  are tridiagonal matrices with  $j^{th}$  row elements as in Table 2.

TABLE 2. The element integrals of the matrices  $M_{000}$  and  $M_{100}$ .

Index Matrix	$j - 1$	$j$	$j + 1$
$j^{th}$ row of $M_{000}$	$\frac{3}{70} h_{j+1}$	$\frac{20}{70} (h_j + h_{j+1})$	$\frac{3}{70} h_{j+1}$
$j^{th}$ row of $M_{100}$	$\frac{17}{70}$	0	$-\frac{17}{70}$

By Substituting the values of  $r_{ji}$  and  $t_{ji}$  from Table 2 in (48) and using the definition of  $\vartheta_{ji}$ , we get the desired consequence.  $\blacksquare$

#### 4. RESULTS AND DISCUSSIONS

Since the main goal of this work is applying hp-cloud method with the stability scheme, most of the discussion (all figures and tables except Table 7) provided here will be about the main stability parameter (30) given by the theorem above. However, only Table 7 sheds some light on the FEM stability parameter given by Lemma 2, this discussion takes a form of comparison with the main stability parameter.

For point nucleus, the relativistic formula is used to compare our results

$$(49) \quad \lambda_{n_r, \kappa} = \frac{mc^2}{\sqrt{1 + \frac{Z^2 \alpha^2}{(n_r - 1 + \sqrt{\kappa^2 - Z^2 \alpha^2})^2}}},$$

where  $\alpha$  is the fine structure constant which has, in atomic unit, the value  $1/c$ , and the quantum number  $n_r$  takes the values  $1, 2, \dots$ . To ease performing the comparison, the exact eigenvalues  $\lambda_{n_r, \kappa}$  and the positive computed eigenvalues are shifted by  $-mc^2$ . All computations are run for the Hydrogen-like Ununoctium ion, where the atomic number and atomic weight for the Ununoctium element are 118 and 294 respectively. Consequently, and since the electron in the Hydrogen-like Ununoctium ion admits relatively large magnitude energies, for better measuring of the approximation accuracy we use the relative error through out all computations. To treat the singularity of the pure Coulomb potential at  $x = 0$ , extended nucleus is assumed to treat the difficulty by modifying the potential to fit the finite nuclear size. The modified Coulomb potential considers another distribution of the charge along the nucleus (in the region  $[0, R]$  where  $R$  is the nucleus radius) and pure Coulomb potential in the rest of domain, where the continuity and the smooth property (at least  $C^1$ ) should be saved for the total modified potential. For the distribution of charge along nucleus, one can consider e.g. uniform or Fermi distributions, in this work we consider uniformly distributed charge.

The boundary conditions are generally treated, i.e. homogeneous Dirichlet conditions are assumed. Note that for better approximation of the eigenstates  $1s_{1/2}$  and  $2p_{1/2}$ , suitable Neumann boundary conditions should also be considered, see [2]. However, here, we do not treat these individuals, instead, general computations are performed to account for the essence of discussion. The general boundary conditions are simply implemented, after coupling with FEM, by omitting the two finite element functions at the lower and upper boundaries.

As discussed before, the computation for the Dirac eigenvalues requires exponential distribution of the nodal points to capture desired behavior of the radial functions near the origin. The following formula is used in the computation below for this purpose

$$(50) \quad x_i = \exp \left( \ln(I_a + \epsilon) + \left( \frac{\ln(I_b + \epsilon) - \ln(I_a + \epsilon)}{n} \right) i \right) - \epsilon, \quad i = 0, 1, 2, \dots, n,$$

where  $n$  is the total number of nodal points and  $\epsilon \in [0, 1]$  is the nodes intensity parameter. The role of  $\epsilon$  is to control the intensity of the nodal points close to origin, as smaller  $\epsilon$  as more nodes are dragged toward the origin, see discussion below. As for other approximation methods, increasing the number of nodal points provides better approximation, but this, of course, on

the account of the computational time. However, we still can obtain good approximation with relatively less time compared with increasing the nodal points if the number of integration points is increased (the same size of the generalized matrices for fixed number of nodal points, where increasing number of integration points means more time is needed for functions evaluation but the same time is used for eigenvalues computation of the generalized system). This never means that we do not need to increase the nodal points so that obtaining more computed eigenvalues and improving the approximation, but to get better rate of convergence with less time, increasing both the numbers of integration points and nodal points is sufficient. Here, in the computation, we fix the number of integration points at  $10 \cdot n$ .

Table 3 shows the approximated energies of the electron in the Hydrogen-like Ununoctium ion obtained using the usual and the stabilized hp-cloud methods, where the dilation parameter is  $\rho_j = 2.2h_{j+1}$  and the nodes intensity parameter is  $\epsilon = 10^{-5}$  with 600 nodes. The clouds are enriched by  $P^t(x) = [1, x(1 - x/2) \exp(-x/2)]$ . In the usual hp-cloud method, the instilled spurious eigenvalues appear for both positive and negative  $\kappa$  (the two shaded values in the fourteenth level of the second and third columns), also the so-called unphysical coincidence phenomenon occurs for the positive  $\kappa$  (the first shaded value in the second column). Note that these spuriousity of both categories are removed by the stability scheme.

TABLE 3. The first computed eigenvalues of the electron in the Hydrogen-like Ununoctium ion using the usual and the stabilized hp-cloud methods for point nucleus.

Level	hp-cloud $\kappa = 2$	hp-cloud $\kappa = -2$	Exact solution $\kappa = -2$	hp-CPG $\kappa = -2$	hp-CPG $\kappa = 2$
1	-1829.630750899	-1829.630750902	-1829.630750908	-1829.628309112	
2	-826.7698136330	-826.7698136329	-826.7683539069	-826.7714785272	-826.7738882959
3	-463.1214970564	-463.1214970566	-463.1183252634	-463.1247150569	-463.1261170024
4	-294.4552367950	-294.4552367952	-294.4509801141	-294.4591541031	-294.4600671778
5	-203.2468937049	-203.2468937047	-203.2419549027	-203.2511517040	-203.2517946674
6	-148.5588260984	-148.5588260983	-148.5534402360	-148.5632453116	-148.5637243357
7	-113.2536099083	-113.2536099084	-113.2479180697	-113.2580871797	-113.2584595495
8	-89.16385480233	-89.16385480237	-89.15794547564	-89.16832365853	-89.16862284813
9	-72.00453396071	-72.00453396065	-71.99846504808	-72.00894720487	-72.00919403005
10	-59.35481340095	-59.35481340100	-59.34862423729	-59.35913470352	-59.35934276227
11	-49.76429096817	-49.76429096819	-49.75800915710	-49.76849047005	-49.76866900765
12	-42.32147184311	-42.32147184312	-42.31511730902	-42.32552373918	-42.32567925216
13	-36.43039621976	-36.43039621984	-36.42398370073	-36.43427738957	-36.43441456989
14	-33.96502895994	-33.96502895893	-31.68173025393	-31.69187884728	-31.69200116063
15	-31.68818961940	-31.68818961935	-27.80813459180	-27.81810976712	-27.81821982418

#### 4.1. Integration of hp-cloud functions.

To approximate the integrals of the weak form in the Galerkin MMs in general, we use Gaussian quadrature rules (namely two-point rule). These techniques are the most used to evaluate the integrals in MMs due to their exact integration of polynomials of degree  $2m_q - 1$ , where

$m_q$  is the number of quadrature points [18]. However, using Gaussian quadrature rules yields integration error when the grids are not coincident with the clouds covers, and thus instabilities and spurious modes start to appear. Also for non-uniform distributed points (the case we assume in this work), Gaussian rules do not pass patch test (fail in consistency). Therefore, stabilizing conforming nodal integration (SCNI) [9] is introduced to overcome these difficulties. The main feature of SCNI is using the divergence theorem to substitute the derivative, i.e. the derivative  $\frac{d}{dx}\Psi^h$  in the sub-domain  $\Omega_j = [x_j, x_{j+1}]$  is replaced by a smooth derivative (averaging derivative)  $\frac{\bar{d}}{dx}\Psi^h$  at  $\hat{x} \in \Omega_j$

$$\frac{d}{dx}\Psi^h(x) \cong \frac{\bar{d}}{dx}\Psi^h(\hat{x}) = \frac{1}{x_{j+1} - x_j} \int_{x_j}^{x_{j+1}} \frac{d}{dx}\Psi^h(x)dx = \frac{\Psi^h(x_{j+1}) - \Psi^h(x_j)}{x_{j+1} - x_j}.$$

This definition helps stabilizing the integration, on the other hand, it saves time in the computation by not calculating the derivative of the cloud functions, thus no need to evaluate  $(M^{-1})' = -M^{-1}M'M^{-1}$  which is expensive to calculate. For integrating and programming the weak form in MMs, [13, 14] are useful.

The cloud shape functions are evaluated at the integration points (digital evaluation), since, practically, it is somehow impossible to write the cloud functions explicitly without matrix inversion. Also, it is not recommended to obtain the inverse of  $M$  directly, instead, LU factorization is better to be used from cost (less time consumption) and numerical stability point of views. Moreover, in MMs generally, to enhance the stability of the computation and to maintain the accuracy (that may be affected or lost due to the round-off error), and to get better conditioning of the matrix  $M$  (lower condition number), the origin should be shifted to the evaluation point [18, 24, 27], i.e.  $x$  is replaced by the transformation  $\bar{x} = x - x_{orig}$ , consequently  $\psi_i(x) = P^t(0)M^{-1}(x)B_i(x)$  where  $M(x) = \sum_{i=1}^n \varphi_i(\frac{x-x_i}{\rho_i})P(x_i - x_{orig})P^t(x_i - x_{orig})$  and  $B_i(x) = \varphi_i(\frac{x-x_i}{\rho_i})P(x_i - x_{orig})$ .

#### 4.2. Enrichment basis functions $P(x)$ .

For the reason discussed before, only intrinsic enrichment,  $P(x)$ , is considered for the computation of the eigenvalues of the Dirac operator. The number and the type of enrichment functions in the basis set  $P(x)$  can be chosen arbitrary for each cloud [19, 32], but for practical reasons (lowering both the condition number of  $M$  and the computational time) we assume  $P(x) = [1, p_1(x)]$ . For the approximation of the Dirac eigenvalues, to enrich the cloud with a suitable basis  $P(x)$ , two main properties should be considered; firstly, and sufficient one, the elements of  $P(x)$  ought to have the continuity properties (continuous with continuous first derivatives) of the space  $\mathcal{H}$  so that for all  $j$ , the cloud  $\psi_j$  is a  $C^1$ -function, provided that  $\varphi_j$  is a  $C^1$ -function. Secondly, global behavior and fundamental characters about the electron motion of the Hydrogen-like ion systems should be embedded in  $P(x)$ . Slater type orbital functions (STOs) and Gaussian type orbital functions (GTOs) provide good description of the electron motion [10, 21]. The quadratic term in the exponent of GTOs causes numerical difficulty, that is, with GTOs the matrix  $M$  rapidly becomes poorly conditioned, this is also what is observed when applying quadratic basis enrichments, see [6]. Consequently, STOs are considered as the

enrichment of the hp-cloud functions, thus  $p_1(x)$  can have, e.g. the following forms

$$\exp(-x), x \exp(-x/2), x(1 - x/2) \exp(-x/2), \dots \text{ etc.}$$

Note that, these functions should be multiplied by normalization parameters, but, computationally, there is no effects of multiplication by these parameters.

Since the global behavior of the eigenstates for Hydrogen-like ions in the relativistic case (Dirac equation) does not differ much from that of the non-relativistic case (Schrödinger equation), one can also assume the solution of the radial Coulomb-Schrödinger equation as an enrichment (see e.g. [22])

$$\mathcal{R}_{n\ell}(x) = \mathcal{N}_{n\ell} (2Zx/na_0)^\ell \mathbf{L}_{n+\ell}^{2\ell+1}(2Zx/na_0) \exp(-Zx/na_0),$$

where  $\mathbf{L}_{n+\ell}^{2\ell+1}(x) = \sum_{k=0}^{n+\ell} \frac{(-1)^k}{k!} \binom{n+3\ell+1}{n+\ell-k} x^k$  is the Laguerre polynomial,  $a_0$  is the Bohr radius,  $n$  is the orbital level, and  $\ell$  is, as defined before, the orbital angular momentum number given to be zero for  $s$ -states, one for  $p$ -states, two for  $d$ -states, ... etc. For a general enrichment, it is, somehow, tedious to apply the above formula for each level  $n$ , instead, good results are still achievable even with, e.g.  $n$  equals the first possible level of the given state (i.e.  $n = 1$  for all  $s$ -states,  $n = 2$  for all  $p$ -states,  $n = 3$  for all  $d$ -states, ... etc.). Moreover, it is also possible to consider enrichment based on the solution of the radial Coulomb-Dirac equation, see e.g. [11], but the above enrichments are simpler from practical point of view. However, in the coming discussion, the enrichment basis  $P^t(x) = [1, x(1 - x/2) \exp(-x/2)]$  is assumed in all computations.

#### 4.3. Dilation Parameter $\rho$ .

The dilation parameter,  $\rho$ , plays crucial role in the approximation accuracy and stability, it serves as the element size in FEM. The parameter  $\rho$  can be chosen fixed or arbitrary, but it is often assumed to be constant for all hp-clouds. In this work, exponentially distributed nodal points are assumed to get enough knowledge of the radial functions near the origin where they oscillate heavily relative to a region away from it, thus we consider

$$\rho_j = \nu \cdot \max\{h_j, h_{j+1}\} = \nu h_{j+1},$$

where the maximum is considered to get sufficient region where the cloud function is defined so that less possibility for singularity of the matrix  $M$  to happen, and  $\nu$  is the dimensionless size of influence domain [27]. Also  $\nu$  for non-uniform mesh can be locally chosen, i.e.  $\nu = \nu_j$ , here we assume fixed  $\nu$  for all nodes. It remains to determine the value/values of  $\nu$  taking into account that  $\rho_j$  should be large enough ( $\nu > 1$ ) to ensure the invertibility of  $M$  (to ensure that any region is covered by at least two clouds). On the other hand,  $\rho_j$  should not be very large to guarantee local character of the approximation. As discussed before (see also Figure 3, the case  $\nu = 1.2$ ), if  $\nu \rightarrow 1$ , then  $\psi_j$  will act as finite element shape function, and thus the features of the hp-clouds are gradually lost, also a very large value of  $\nu$  makes  $\psi_j$  to behave like polynomial of higher degree (see Figure 3, the case  $\nu = 4$ ). To conclude,  $\nu$  should be chosen moderately and such that it guarantees that no integration point is covered by only one cloud [27, 32].

The optimal choice of  $\nu$  can be determined individually for each problem by carrying out numerical experiments. In [30, 44], it is shown that  $\nu \in [2, 3]$  provides nice results for elasticity problem. For the computation of the Dirac eigenvalues with the stability scheme, for  $\nu \in [2.2, 2.7]$  good results are obtained and the spurious eigenvalues are completely eliminated. Also as small as  $\nu$  in  $[2.2, 2.7]$  as better approximation is obtained, see Table 4.

TABLE 4. The first computed eigenvalues of the electron in the Hydrogen-like Ununoctium ion for  $\kappa = -2$  for point nucleus with different values of  $\nu$ , where  $n = 600$  and  $\epsilon = 10^{-5}$  are used.

Level	$\nu = 2.0$	$\nu = 2.2$	$\nu = 2.5$	$\nu = 2.7$	Exact solution
1	-1829.6287	-1829.6283	-1829.6276	-1829.6270	-1829.6307
2	-826.77119	-826.77147	-826.77197	-826.77233	-826.76835
3	-463.12417	-463.12471	-463.12567	-463.12638	-463.11832
4	-294.45850	-294.45915	-294.46033	-294.46120	-294.45098
5	-203.25046	-203.25115	-203.25244	-203.25340	-203.24195
6	-148.56255	-148.56324	-148.56460	-148.56562	-148.55344
7	-113.25741	-113.25808	-113.25949	-113.26054	-113.24791
8	-89.167688	-89.168323	-89.169756	-89.170831	-89.157945
9	-72.008358	-72.008947	-72.010396	-72.011489	-71.998465
10	-59.358602	-59.359134	-59.360592	-59.361700	-59.348624
11	-49.768025	-49.768490	-49.769950	-49.771070	-49.758009
12	-42.325133	-42.325523	-42.326981	-42.328113	-42.315117
13	-36.433970	-36.434277	-36.435728	-36.436870	-36.423983
14	-31.691663	-31.691878	-31.693318	-31.694472	-31.681730
15	-27.817992	-27.818109	-27.819533	-27.820699	-27.808134

For the first five eigenvalues in Table 4, we study the convergence behavior of the approximation in Figure 4.

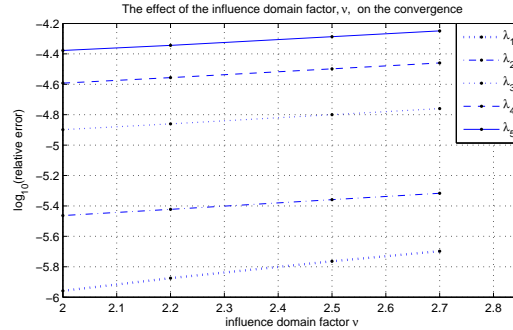


FIGURE 4. Studying the convergence rate with respect to the influence domain factor  $\nu$ . The comparison is carried out for the first five eigenvalues in Table 4.

It is clear how the smaller  $\nu$  gives better approximation. One argues, as it is clear from the figure, that  $\nu$  can be e.g. some value less than 2 to achieve better rate of convergence, however,

this will be on the account of spuriousity elimination (the cloud is not stretched enough to capture the desired behavior of the approximated solution) and on the account of the invertibility of the matrix  $M$  (for small  $\nu$  some regions are covered with one cloud). However, as in FEM, one can apply h-refinement in hp-cloud method (see e.g. [16, 44]), this can be done by decreasing the value of the dilation parameter  $\rho_j$  (keeping  $\nu$  fixed and making  $h_{j+1}$  smaller), thus as  $\rho_j$  getting smaller then more clouds of smaller size are added.

The intensity of the exponentially distributed nodal points near the origin has an influence on the convergence rate of the approximation. The intensity of the nodes near the origin or away from it is controlled by the nodes intensity parameter,  $\epsilon$ , via formula (50). As smaller value of  $\epsilon$  is considered as more concentration of nodes near the origin is obtained, see Figure 5 the graph to the left.

Table 5 shows the computation of the eigenvalues with different values of  $\epsilon$  with 600 nodal points. The computation with  $\epsilon$  smaller than  $10^{-7}$  is almost the same as of  $\epsilon = 10^{-7}$ , thus it is not required to study smaller values of  $\epsilon$  than  $\epsilon = 10^{-7}$ .

TABLE 5. The first computed eigenvalues of the electron in the Hydrogen-like Ununoctium ion for  $\kappa = -2$  for point nucleus with different values of  $\epsilon$ , where  $n = 600$  and  $\nu = 2.2$  are used.

Level	$\epsilon = 10^{-4}$	$\epsilon = 10^{-5}$	$\epsilon = 10^{-6}$	$\epsilon = 10^{-7}$	Exact solution
1	-1829.6289	-1829.6283	-1829.6280	-1829.6280	-1829.6307
2	-826.77073	-826.77147	-826.77170	-826.77173	-826.76835
3	-463.12322	-463.12471	-463.12517	-463.12523	-463.11832
4	-294.45726	-294.45915	-294.45973	-294.45981	-294.45098
5	-203.24904	-203.25115	-203.25180	-203.25188	-203.24195
6	-148.56101	-148.56324	-148.56393	-148.56402	-148.55344
7	-113.25578	-113.25808	-113.25879	-113.25888	-113.24791
8	-89.165992	-89.168323	-89.169039	-89.169131	-89.157945
9	-72.006610	-72.008947	-72.009662	-72.009755	-71.998465
10	-59.356811	-59.359134	-59.359844	-59.359936	-59.348624
11	-49.766195	-49.768490	-49.769189	-49.769279	-49.758009
12	-42.323268	-42.325523	-42.326208	-42.326296	-42.315117
13	-36.432073	-36.434277	-36.434943	-36.435030	-36.423983
14	-31.689734	-31.691878	-31.692524	-31.692607	-31.681730
15	-27.816033	-27.818109	-27.818732	-27.818812	-27.808134

In Figure 5, the first computed eigenvalues of Table 5 are studied. It is clear that as  $\epsilon$  gets larger (up to some limit) the better approximation is obtained. However, as mentioned before, the rate of convergence is almost the same when  $\epsilon \in (0, 10^{-7})$  ( $\epsilon = 0$  is excluded to avoid  $\log(0)$  when extended nucleus is assumed), also  $\epsilon$  does not admit relatively large values in order to get enough nodes close to origin, where the radial functions oscillate relatively more, without increasing the total nodal points. Therefore, the most appropriate values of  $\epsilon$ , which provides good results, are somewhere in  $[10^{-6}, 10^{-4}]$ .



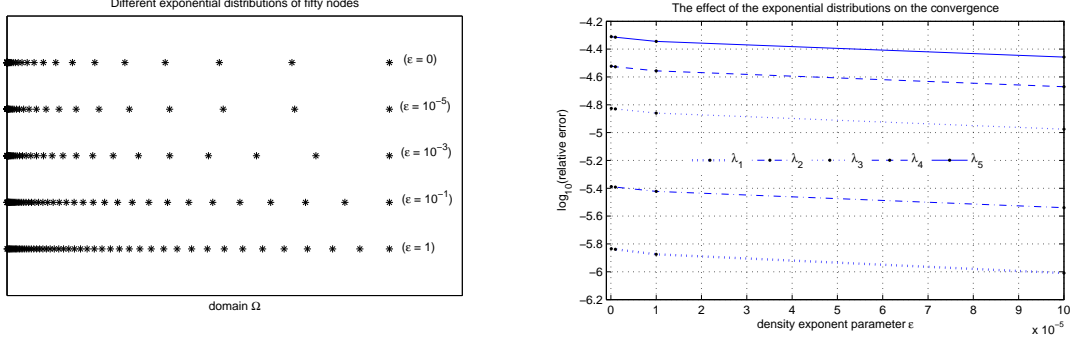


FIGURE 5. To the left, different exponentially distributed nodal points are plotted using the mesh formula (50). To the right, the effect of nodes intensity near the origin on the convergence rate, the comparison is carried out for the first five eigenvalues in Table 5.

The approximation of the stabilized hp-cloud scheme with different numbers of nodal points is given in Table 6. The rate of convergence of the corresponding first five eigenvalues is studied in Figure 6, where  $h$  is the maximum of all distances between the adjacent nodes which equals to  $h_n = x_n - x_{n-1}$ , the distance between the last two nodes for exponentially distributed nodes.

TABLE 6. The first computed eigenvalues of the electron in the Hydrogen-like Ununoctium ion for  $\kappa = -2$  for point nucleus with different number of nodes, where  $\nu = 2.2$  and  $\epsilon = 10^{-5}$  are used.

Level	$n = 200$	$n = 400$	$n = 600$	$n = 800$	$n = 1000$	Exact solution
1	-1829.5628	-1829.6224	-1829.6283	-1829.6297	-1829.6302	-1829.6307
2	-826.82670	-826.77726	-826.77147	-826.76987	-826.76923	-826.76835
3	-463.23292	-463.13630	-463.12471	-463.12146	-463.12016	-463.11832
4	-294.59147	-294.47367	-294.45915	-294.45503	-294.45336	-294.45098
5	-203.39386	-203.26721	-203.25115	-203.24654	-203.24466	-203.24195
6	-148.70878	-148.58009	-148.56324	-148.55835	-148.55635	-148.55344
7	-113.40170	-113.27527	-113.25808	-113.25304	-113.25096	-113.24791
8	-89.306709	-89.185557	-89.168323	-89.163201	-89.161076	-89.157945
9	-72.139617	-72.026008	-72.008947	-72.003802	-72.001653	-71.998465
10	-59.480154	-59.375861	-59.359134	-59.354006	-59.351849	-59.348624
11	-49.878353	-49.784751	-49.768490	-49.763410	-49.761256	-49.758009
12	-42.423104	-42.341207	-42.325523	-42.320517	-42.318374	-42.315117
13	-36.518814	-36.449288	-36.434277	-36.429365	-36.427242	-36.423983
14	-31.762955	-31.706134	-31.691878	-31.687081	-31.684984	-31.681730
15	-27.875610	-27.831538	-27.818109	-27.813442	-27.811376	-27.808134

The lack of error estimates of the Dirac operator due to the boundedness problem (neither bounded from above nor from below) results in incomplete picture about the convergence analysis. Nevertheless, from Figure 6, the convergence rates of the approximation of the first five

eigenvalues,  $\lambda_1, \lambda_2, \dots, \lambda_5$ , are nearly 3.09, 2.66, 2.62, 2.59, and 2.56 respectively, which takes a slight decreasing pattern as we go higher in the spectrum levels, see the corresponding table.

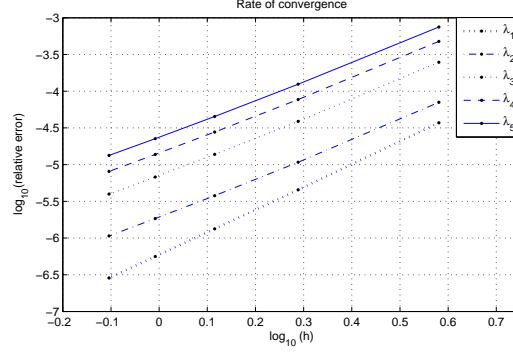


FIGURE 6. Study the convergence rate of the first computed five eigenvalues in Table 6.

With the stability parameter  $\tau^{FEM}$ , the computation is presented in Table 7. The computation is obtained with 600 nodal points at  $\nu = 1.1$  and  $\epsilon = 10^{-5}$ . The result is compared with the same stability scheme but with the stability parameter  $\tau$  at the same parameters but  $\nu = 2.2$ , the comparison is also obtained in the non-relativistic limit (very large  $c$ ).

TABLE 7. The first computed eigenvalues of the electron in the Hydrogen-like Ununoctium ion for  $\kappa = -2$  for point nucleus using the stabilized scheme with the main stability parameter  $\tau$  and the finite element stability parameter  $\tau^{FEM}$ .

Level	The speed of light			100×The speed of light		
	$\tau$	$\tau^{FEM}$	Exact values	$\tau$	$\tau^{FEM}$	Exact values
1	-1829.6283	-1829.6304	-1829.6307	-1740.2372	-1740.4777	-1740.5080
2	-826.77147	-826.76993	-826.76835	-773.73860	-773.57259	-773.56033
3	-463.12471	-463.12174	-463.11832	-435.46054	-435.14787	-435.12752
4	-294.45915	-294.45551	-294.45098	-278.88245	-278.49775	-278.48144
5	-203.25115	-203.24715	-203.24195	-193.82362	-193.39522	-193.38978
6	-148.56324	-148.55905	-148.55344	-142.53145	-142.07261	-142.08222
7	-113.25808	-113.25377	-113.24791	-109.23625	-108.75140	-108.78165
8	-89.168323	-89.163916	-89.157945	-86.404375	-85.894382	-85.950912
9	-72.008947	-72.004478	-71.998465	-70.067886	-69.534118	-69.620219
10	-59.359134	-59.354644	-59.348624	-57.975599	-57.420335	-57.537357
11	-49.768490	-49.764010	-49.758009	-48.773149	-48.197640	-48.347352
12	-42.325523	-42.321064	-42.315117	-41.606088	-41.009232	-41.195370
13	-36.434277	-36.429826	-36.423983	-35.913753	-35.292096	-35.520492
14	-31.691878	-31.687405	-31.681730	-31.315908	-30.664671	-30.942291
15	-27.818109	-27.813579	-27.808134	-27.547311	-26.861865	-27.195369

As it is noted from Table 7, the convergence property with  $\tau^{FEM}$  is slightly better. Unfortunately, the approximation with  $\tau^{FEM}$  seems to behave strangely at the end of the spectrum, that

is, only the spectrum tail has the following behavior (the tail of the spectrum of the computation in Table 7 with  $\tau^{FEM}$  for the relativistic case)

$\lambda_+ - mc^2$	$\lambda_- + mc^2$
207072481.0215	-215565247.3448
211429663.4158*	-220006205.1800*
226003907.3130	-235294474.7992
231896256.0483*	-241138935.9851*
246890583.9362	-257366374.4374
257292411.7094*	-267386241.2969*
267659710.2673*	-279193268.7275*
291928112.6166	-303237209.5231
296228215.8873*	-308029351.9019*

This behavior occurs only for few values at the end of the spectrum, and no such effect is revealed in the rest of the spectrum. Up to our knowledge, the values marked with \* might be spurious eigenvalues for some unknown origins in higher levels, which, in calculating the correlation energy, seem to have not any significant effect.

Table 8 shows the computation of the eigenvalues of the Dirac operator for Hydrogen-like Ununoctium ion with  $\kappa = -2$ . The computation is for extended nucleus obtained using the stability approach, where the first and the last computed eigenvalues are presented. The number of nodes used is 1000, also the used values of  $\nu$  and  $\epsilon$  are respectively 2.2 and  $10^{-5}$ .

## Conclusion.

The scheme developed in this work, hp-CPG, for stabilizing the hp-cloud approximation for solving the single-electron Dirac-Coulomb operator ensures complete treatment of the spuriousity problem. The scheme depends strongly on the derived stability parameter  $\tau$ , which is simple to implement and applicable for general finite basis functions. The elimination of the spurious eigenvalues is affected also by the influence domain factor  $\nu$ , for  $\nu$  less than 2, spuriousity starts to appear. The convergence rate is high for the first energy levels, while it decreases slowly as the level gets higher. Whereas, comparable to the finite element stability approach [2], the scheme convergence rate is lower. Also, which can be regarded as the main disadvantage of MMs computation in general, hp-cloud method is more expensive due to the time consumption in evaluating the shape function which demands more integration point as  $\nu$  gets larger to obtain the desired accuracy. The number of integration point used here is ten times number of nodal points (this large number of integration points is assumed in order to study the effects of the other parameters in a comparative point of view), which can be made smaller, i.e.  $\nu \geq 2$  is enough to get sufficient accuracy.

TABLE 8. The first and the last computed eigenvalues of the electron in the Hydrogen-like Ununoctium ion for  $\kappa = -2$  for extended nucleus using the stabilized scheme.

Level	$\lambda_+ - mc^2$	$\lambda_- + mc^2$	Level	$\lambda_+ - mc^2$	$\lambda_- + mc^2$
1	-1829.630099296	-2.434417024833	956	586688854.9879	-592440657.5171
2	-826.7693836687	-2.627617735663	957	598438233.4986	-604235496.3134
3	-463.1204703095	-2.797844649762	958	610919226.3899	-616906339.6739
4	-294.4537598806	-2.957820323769	959	623291095.2201	-629316989.3797
5	-203.2451112716	-3.112227360954	960	636480181.4813	-642726428.9931
6	-148.5568310625	-3.263408080529	961	649524826.4034	-655799753.0246
7	-113.2514598678	-3.412742089389	962	663483591.3527	-670016495.9307
8	-89.16158600002	-3.561138820860	963	677258040.9295	-683804920.4801
9	-72.00216968256	-3.709254718702	964	692056051.2167	-698907640.1176
10	-59.35236884621	-3.857601123902	965	706625519.7561	-713470210.1966
11	-49.76177611950	-4.006600112632	966	722341703.9586	-729549529.5797
12	-42.31889320986	-4.156612122006	967	737781471.5140	-744953276.6295
13	-36.42775793119	-4.307947863723	968	754505800.5837	-762114239.5911
14	-31.68549413213	-4.460872692773	969	770903696.8948	-778435989.9532
15	-27.81188079379	-4.615608997468	970	788739250.6668	-796801160.7705
16	-24.60715078621	-4.772339706105	971	806198985.1845	-814129982.6368
17	-21.92579810728	-4.931213787881	972	825264528.2332	-833843359.2405
18	-19.65981495410	-5.092353196094	973	843910220.2386	-852283956.3394
19	-17.72767091768	-5.255860198286	974	864343472.0411	-873515941.8428
20	-16.06689248232	-5.421824189525	975	884325905.7234	-893193487.1967
21	-14.62895927631	-5.590327472124	976	906287797.8413	-916147241.8477
22	-13.37572611330	-5.761449842514	977	927793189.6390	-937214464.1559
23	-12.27687110094	-5.935272041930	978	951473602.6651	-962134060.6197
24	-11.30804689661	-6.111878218067	979	974736078.1642	-984781962.7117
25	-10.44952215915	-6.291357562437	980	1000361933.873	-1011962889.837
26	-9.685170122048	-6.473805266356	981	1025681563.220	-1036437526.155
27	-9.001706528736	-6.659322921776	982	1053528920.945	-1066240230.486
28	-8.388109077412	-6.848018469445	983	1081298213.911	-1092869973.210
29	-7.835170608265	-7.040005799103	984	1111711637.956	-1125737288.414
30	-7.335151949937	-7.235404092542	985	1142455141.979	-1154979024.500
31	-6.881509811941	-7.434337004637	986	1175881200.913	-1191458619.345
32	-6.468681741462	-7.636931764649	987	1210315776.667	-1223979724.299
33	-6.091914867255	-7.843318267751	988	1247366017.754	-1264753730.099
34	-5.747128531017	-8.053628212296	989	1286494208.919	-1301585190.310
35	-5.430803353698	-8.267994317084	990	1328074902.403	-1347514563.183
36	-5.139891080678	-8.486549638106	991	1373330615.013	-1390354085.681
37	-4.871740872106	-8.709426988262	992	1420940894.294	-1442573015.641
38	-4.624038699727	-8.936758453401	993	1474405770.317	-1494428385.378
39	-4.394757252718	-9.168674990411	994	1530930196.971	-1554661710.974
40	-4.182114320607	-9.405306088338	995	1595537987.175	-1621361454.883
41	-3.984538053675	-9.646779469269	996	1667868144.599	-1693349701.469
42	-3.800637833043	-9.893220807513	997	1746516931.180	-1787808061.719
43	-3.629179737774	-10.14475343997	998	1858171146.415	-1885927735.358
44	-3.469065800899	-10.40149804032	999	1944896072.579	-2040151500.838
45	-3.319316399200	-10.66357222412	1000	2551096858.208	-2992548052.333

## REFERENCES

- [1] E. Ackad and M. Horbatsch, *Numerical solution of the Dirac equation by a mapped fourier grid method*, J. Phys. A: Math. Gen., 38(2005), pp. 3157-3171.
- [2] H. Almanasreh, S. Salomonson, and N. Svanstedt, *Stabilized finite element method for the radial Dirac equation*, (submitted), URL <http://arxiv.org/abs/1111.6263>.
- [3] R. C. Almeida and R. S. Silva, *A stable Petrov-Galerkin method for convection-dominated problems*, Comput. Methods Appl. Mech. Engng., 140(1997).
- [4] S. N. Atluri and S. Shen, *The meshless local Petrov-Galerkin (MLPG) method: A simple and less-costly alternative to the finite element and boundary element methods*, CMES, 3(2002), pp. 11-51.
- [5] T. Belytschko, D. Organ, and Y. Krongauz, *A coupled finite element-element-free Galerkin method*, Comput. Mech., 17(1995), pp. 186-195.
- [6] T. Belytschko, Y. Krongauz, D. Organ, M. Fleming, and P. Krysl, *Meshless methods: An overview and recent developments*, Comput. Methods Appl. Mech. Engng., 139(1996), pp. 3-47.
- [7] A. N. Brooks, *A Petrov-Galerkin finite element formulation for convection dominated flows*, Thesis for the degree of Doctor of Philosophy, California Institute of Technology, California, 1981.
- [8] A. N. Brooks and T. J. R. Hughes, *Streamline Upwind/Petrove-Galerkin formulations for convection dominated flows with particular emphasis on the incompressible Navier-Stokes equations*, Comput. Methods Appl. Mech. Engng., 32(1982).
- [9] J. S. Chen, C. T. Wu, S. Yoon, and Y. You, *A stabilized conforming nodal integration for Galerkin mesh-free methods*, Int. J. Numer. Methods Engng., 50(2001), pp. 435-466.
- [10] J. S. Chen, W. Hu, and M. A. Puso, *Orbital hp-clouds for solving Schrödinger equation in quantum mechanics*, Comput. Methods Appl. Mech. Engng., 196(2007), pp. 3693-3705.
- [11] H. Ciftci, R. L. Hall, and N. Saad, *Iterative solutions to the Dirac equation*, Phys. Rev. A, 72(2005).
- [12] P. A. B. De Sampaio, *A Petrov-Galerkin/modified operator formulation for convection-diffusion problems*, Int. J. Numer. methods Engng., 30(1990).
- [13] J. Dolbow and T. Belytschko, *An introduction to programming the meshless element free Galerkin method*, Arch. Comput. Method E., 5(1998), pp. 207-241.
- [14] J. Dolbow and T. Belytschko, *Numerical integration of the Galerkin weak form in meshfree methods*, Comput. Mech., 23(1999), pp. 219-230.
- [15] C. A. Duarte and J. T. Oden, *H-p clouds—An h-p meshless method*, Numer. Meth. Part. D. E., 12(1996), pp. 673-705.
- [16] C. A. Duarte and J. T. Oden, *An h-p adaptive method using clouds*, Comput. Methods Appl. Mech. Engng., 139(1996), pp. 237-262.
- [17] T. Fries and H. Matthies, *A review of Petrov-Galerkin stabilization approaches and an extension to meshfree methods*, Institute of scientific computing, Technical University Braunschweig, Brunswick, Germany.
- [18] T. Fries and H. Matthies, *Classification and overview of Meshfree Methods*, Institute of scientific computing, Technical University Braunschweig, Brunswick, Germany.
- [19] O. Garcia, E. A. Fancello, C. S. de Barcellos, and C. A. Duarte, *hp-Clouds in Mindlin's thick plate model*, Int. J. Numer. methods Engng., 47(2000), pp. 1381-1400.
- [20] M. Griesemer and J. Lutgen, *Accumulation of Discrete Eigenvalues of the Radial Dirac Operator*, J. Funct. Anal., 162(1999).

- [21] W. J. Hehre, L. Radom, P. Schleyer, and J. Pople, *Ab initio molecular orbital theory*, John Wiley & Sons, New York, 1986.
- [22] W. T. Hill and C. H. Lee, *Light-Matter interaction: Atoms and molecules in external fields and nonlinear optics*, Wiley-VCH Verlag GmbH & Co. KGaA, Weinheim, 2007.
- [23] A. Huerta and S. Fernández-Méndez, *Coupling element free Galerkin and finite element methods*, ECCOMAS, Barcelona, 2000.
- [24] A. Huerta and S. Fernández-Méndez, *Enrichment and coupling of the finite element and meshless methods*, Int. J. Numer. methods Engng., 48(2000), pp. 1615-1636.
- [25] S. Idelsohn, N. Nigro, M. Storti, and G. Buscaglia, *A Petrov-Galerkin formulation for advection-reaction-diffusion problems*, Comput. Methods Appl. Mech. Engng., 136(1996).
- [26] Y. Krongauz and T. Belytsko, *Enforcement of essential boundary conditions in meshless approximations using finite elements*, Comput. Methods Appl. Mech. Engng., 131(1996), pp. 133-145.
- [27] C. V. Le, *Novel numerical procedures for limit analysis of structures: Mesh-free methods and mathematical programming*, Ph.D thesis, University of Sheffield, England, 2009.
- [28] H. Lin and S. N. Atluri, *Meshless local Petrov-Galerkin (MLPG) method for convection-diffusion problems*, CMES, 1(2000), pp. 45-60.
- [29] I. Lindgren, S. Salomonson, and B. Åsén, *The covariant-evolution-operator method in bound-state QED*, Physics Reports, 389(2004), pp. 161-261.
- [30] G. R. Liu, *Mesh free methods: Moving beyond the finite element method*, CRC press, 2003.
- [31] Y. Y. Lu, T. Belytschko, and L. Gu, *A new implementation of the element free Galerkin method*, Comput. Methods Appl. Mech. Engng, 113(1994), pp. 397-414.
- [32] P. de T. R. Mendonça, C. S. de Barcellos, A. Duarte, *Investigations on the hp-cloud method by solving Timoshenko beam problems*, Comput. Mech., 25(2000), pp. 286-295.
- [33] P. J. Mohr, G. Plunien, and G. Soff, *QED corrections in heavy atoms*, Physics Reports, 293(1998), pp. 227-369.
- [34] G. Mur, *On the causes of spurious solutions in electromagnetics*, Electromagnetic, 22(2002), pp. 357-367.
- [35] V. P. Nguyen, T. Rabczuk, S. Bordas, and M. Duflot, *Meshless methods: A review and computer implementation aspects*, Math. Comput. Simulat., 79(2008), pp. 763-813.
- [36] H. Noguchi, T. Kawashima, and T. Miyamura, *Element free analyses of shell and spatial structures*, Int. J. Numer. methods Engng., 47(2000), pp. 1215-1240.
- [37] G. Pestka, *Spurious roots in the algebraic Dirac equation*, Chem. Phys. Lett. 376(2003), pp. 659-661.
- [38] L. Rosenberg, *Virtual-pair effects in atomic structure theory*, Phys. Rev. A, 39(1989), pp. 4377-4386.
- [39] W. Schroeder and I. Wolf, *The origin of spurious modes in numerical solutions of electromagnetic field eigenvalue problems*, IEEE Tran. on Micr. Theory and Tech., 42(1994), pp. 644-653.
- [40] V. M. Shabaev, *Two-time Green's function method in quantum electrodynamics of high-Z few-electron atoms*, Physics Reports, 356(2002), pp. 119-228.
- [41] V. M. Shabaev, I. I. Tupitsyn, V. A. Yerokhin, G. Plunien, and G. Soff, *Dual kinetic balance approach to basis-set expansions for the Dirac equation*, Phys. Rev. Lett., 93(2004).
- [42] B. Thaller, *The Dirac equation*, Springer-Verlag, Berlin, 1993.
- [43] I. I. Tupitsyn and V. M. Shabaev, *Spurious states of the Dirac equation in a finite basis set*, Optika i Spektroskopiya, 105(2008), pp. 203-209.

- [44] Y. You, J. S. Chen, and H. Lu *Filters, reproducing kernel, and adaptive meshfree method*, Comput. Mech., 31(2003), pp. 316-326.
- [45] X. Zhang, X. Liu, M. Lu, and Y. Chen, *Imposition of essential boundary conditions by displacement constraint equations in meshless methods*, Commun. Numer. Meth. Engng., 17(2001), pp. 165-178.
- [46] S. Zhao, *On the spurious solutions in the high-order finite difference methods for eigenvalue problems*, Comput. Methods Appl. Mech. Engng., 196(2007), pp. 5031-5046.
- [47] C. Zuppa, *Modified Taylor reproducing formulas and h-p clouds*, Math. Comput., 77(2008), pp. 243-264.